Widefield Spectral Monitoring of Nanometer Distance Changes in DNA-Templated Plasmon Rulers

Laurent Lermusiaux, Vincent Maillard, and Sébastien Bidault*

ESPCI ParisTech, PSL Research University, CNRS, INSERM, Institut Langevin, 1 rue Jussieu, F-75005 Paris, France

ABSTRACT The nanometer-scale sensitivity of electromagnetic plasmon coupling allows the translation of minute morphological changes in nanostructures into macroscopic optical signals. We demonstrate here a widefield spectral analysis of 40 nm diameter gold nanoparticle (AuNP) dimers, linked by a short DNA double strand, using a low-cost color CCD camera and allowing a quantitative estimation of interparticle distances in a 3−20 nm range. This analysis can be extended to lower spacings and a parallel monitoring of dimer orientations by performing a simple polarization analysis. Our measurement approach is calibrated against confocal scattering spectroscopy using AuNP dimers that are distorted from a stretched geometry at low ionic strength to touching particles at high salt concentrations. We then apply it to identify dimers featuring two different conformations of the same DNA template and discuss the parallel colorimetric sensing of short sequence-specific DNA single strands using dynamic plasmon rulers.

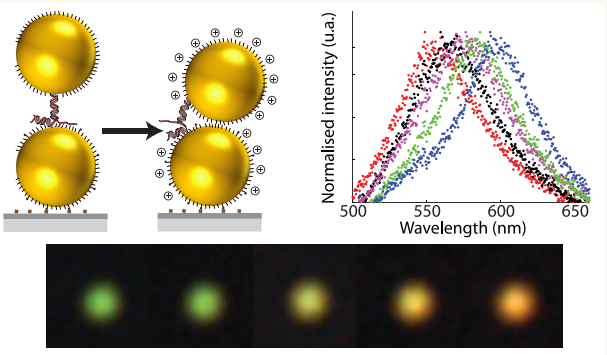

KEYWORDS: plasmon ruler · DNA self-assembly · dynamic nanostructures · widefield spectroscopy · darkfield microscopy · colorimetric sensing

The distance-dependent plasmon resonances of gold nanoparticle (AuNP) groupings have allowed the development of biochemical colorimetric sensors[1−3] and molecular rulers.[4,5] Individual AuNP dimers are particularly attractive to optically monitor single biochemical events (such as the cutting, shrinking, or bending of oligonucleotides and proteins) in order to follow conformational changes in biomolecules[6−9] or to sense specific analytes down to femtomolar concentrations.[10−14] Indeed, the relationship between the interparticle distance and the longitudinal plasmon resonance of the dimer, as calibrated using confocal scattering spectroscopy and expected from electrodynamic calculations,[5,15] is sensitive at the nanometer scale for distances lower than the particle radii.[16]

Another appealing feature of gold nanoparticle groupings is that, for AuNPs with diameters larger than 30 nm, they are easily visible by eye or with a low-cost color CCD detector in darkfield microscopy, using a simple white light excitation.[4] Furthermore, single particles, dimers, and multimers can easily be discriminated in this configuration, allowing the parallel analysis of dimer formation[4,5,11] and disassembly,[6,7,14] as well as complex clustering mechanisms in membranes.[17−19] In this report, we demonstrate that darkfield imaging can also provide a quantitative estimation of interparticle distances and distinguish AuNP dimers exhibiting two different conformations of the same DNA linker.

In practice, purified suspensions of 40 nm gold particle dimers are obtained using electrophoretic separation. These dimers feature preferentially one DNA linker due to a minimization of the oligonucleotide surface coverage. A hairpin loop on the DNA scaffold allows it to switch between two conformations as we recently verified in 8 nm diameter AuNP dimers.[20] By introducing these AuNP groupings in homemade microfluidic chambers, we can image several tens of dimers in parallel using darkfield microscopy, with a sample purity reaching

* Address correspondence to sebastien.bidault@espci.fr.

Received for review December 5, 2014 and accepted January 7, 2015.

Published online January 07, 2015
10.1021/nn506947g

80%. To calibrate the spectral response measured on a color CCD camera with respect to confocal scattering spectroscopy and interparticle distances, we analyze the conformational change of dimers when modifying the local ionic strength. We observe two distortion scenarios depending on the incubation kinetics at high salt concentrations: the dimers can reach touching or interpenetrating surface chemistries of the two gold particles.

This experimental method allows us to provide a widefield estimation of interparticle distances and dimer orientations, as well as a discrimination between dimers with an open or closed hairpin loop. It also provides information on the stability and sensitivity of AuNP dimers with respect to the local ionic strength. We discuss these parameters that are essential for the applicability of dynamic plasmon rulers in colorimetric sensing, by optically monitoring the opening and closing of the DNA hairpin loop in AuNP dimers when introducing the complementary nucleotide sequences.

RESULTS AND DISCUSSION

Synthesis and Purification of AuNP Dimers. Agarose gel electrophoresis is a powerful technique to purify gold nanoparticles, with diameters lower than 20 nm, covalently attached to a known number of thiolated DNA single strands[21] and, after hybridization of complementary sequences, of well-defined 2D and 3D AuNP groupings.[22−25] By passivating the particle surface with short thiolated ethylene glycol oligomers[5] and lengthening the grafted DNA with extra single strands,[23] this approach can be extended to 40 nm diameter gold particles.[15] However, the added strands, used to effectively lengthen the DNA grafted on the AuNP, strongly increase the cost and reduce the yield of the assembly process. Here, we propose a simplified approach to produce 40 nm AuNP dimers featuring preferentially a single DNA double-stranded linker. In practice, we reduce the amount of thiolated DNA strands, left to incubate with the AuNPs, in order to only produce dimers after hybridization of particles with complementary single-strand sequences. To remove all unreacted thiolated DNA strands, or oligonucleotides electrostatically attached to the particle surface,[26] we purify the functionalized AuNPs in a first electrophoresis step (shown in Figure S1 of the Supporting Information, SI). Furthermore, the electrostatic attachment of the thiolated DNA strands on the particles is minimized by adding a large excess of a 100 bases long polythymine strand in the reaction mix.

Figure 1a shows the agarose gel purification of 40 nm AuNP groupings, linked by short DNA scaffolds containing two 50 bp DNA double strands for different DNA concentrations and for two reaction times (12 h for columns 7−10 and 120 h for columns 3−6). Columns 1 and 2 correspond to reference 40 nm AuNPs with the two surface chemistries used here: a thiolated ethylene glycol oligomer (column 1) and a mix of this ligand and a longer thiolated ethylene glycol oligomer featuring a biotin moiety to graft one AuNP of the dimers on the functionalized glass slides of the microfluidic chamber.[15] The longer biotinylated ligand induces an increase of the AuNP hydrodynamic volume and, thus, a lower electrophoretic mobility.

As described in a previous report,[20] the DNA scaffold features two 50 bp DNA double strands: one, used to link the particles of the dimer, is perpendicular to the dimer axis; the second, parallel to the dimer axis, contains a hairpin loop that is open in this double-stranded configuration. This scaffold is built using three DNA single strands: a 5′ trithiolated 104 bases long **S** strand contains the stem-loop (20 bp stem and 4 bases long loop); a 3′ trithiolated 50 bases-long **C** strand that is complementary to the 3′ end of **S**; and an 80 bases long **T** strand that hybridizes with the stem-loop of **S** and features a 30 bases overhang to be removed when introducing its complementary sequence (see Figure S1 for details). All DNA sequences and the geometry of the DNA scaffold are given in SI. We use trithiol moieties instead of monothiol groups on the DNA strand to optimize the enthalpic stability of the DNA−AuNP link.[6,15,27] The DNA-functionalized AuNPs, used to form groupings, are obtained by incubating particles with **S**, **C**, or **S**+**T** (strands hybridized prior to the conjugation). Samples purified in columns 3−6 are obtained with the same functionalized AuNPs (**C** and **S**+**T**) incubated in 40 mM NaCl than samples in columns 7−10 but for a 10× longer incubation time. The DNA concentrations are progressively increased by a factor of 2 between columns 3 (respectively 7) and 4 (respectively 8); 4 (respectively 8) and 5 (respectively 9); as well as 5 (respectively 9) and 6 (respectively 10). The initial excess DNA concentration in lane 3, with respect to the AuNP concentration, is 5× for **S**+**T** and 12.5× for **C**. With 8 nm particles (for which the DNA coverage can be estimated in electrophoresis), a 5× DNA excess corresponds preferentially to AuNPs featuring one strand per particle.[20]

The fastest band in Figure 1a corresponds to unreacted AuNPs. The electrophoretic mobility of unreacted particles is similar (columns 3−4 and 7−8) or lower (columns 5−6 and 9−10) than the reference lanes. This result, which is also observed during the initial purification of the monomers (Figure S1), indicates the increased average number of thiolated DNA strands attached per particle for larger DNA concentrations. The second fastest band corresponds to assembled AuNP dimers. This is verified by analyzing these samples in cryo-electron microscopy images, as shown on Figure 1b and was discussed in previous reports.[6,15] Bands that are slower than the dimer band correspond to larger groupings: trimers, quadrimers, *etc.*

We observe that the relative density and the electrophoretic mobility of the dimer bands change when we modify the DNA concentration and, therefore, the

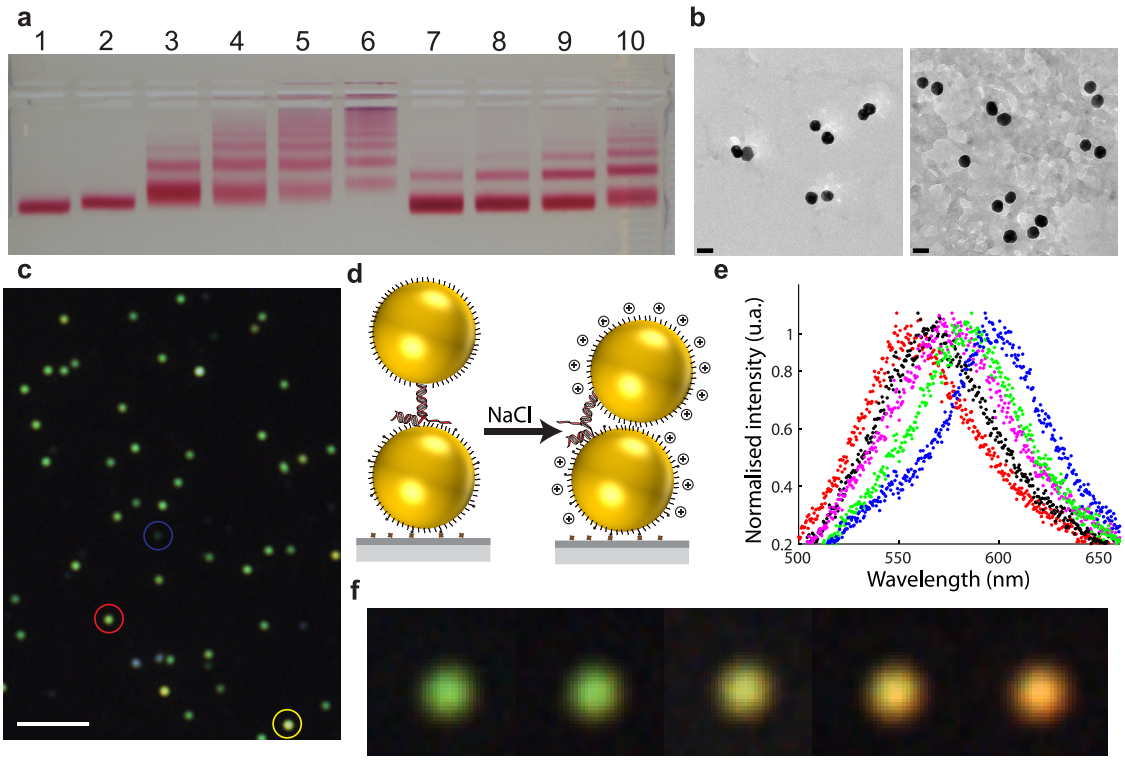

Figure 1. (a) Electrophoretic purification of 40 nm AuNP dimers featuring an open hairpin loop. Lanes 1 and 2 correspond to reference samples with isolated particles featuring the two different surface chemistries. Lanes 3−6 and 7−10 correspond to the same sample concentrations but with a 10× longer incubation time for 3−6. See text for details. (b) Examples of cryo-EM images obtained with the second fastest band of lane 7 (scale bar is 50 nm). (c) Darkfield image of dimers from lane 7 after incubation in Neutravidin-coated microfluidic chambers (scale bar is 5 μm). The typical response of a dimer is circled in red, compared to a single 40 nm AuNP (blue) and a larger grouping (yellow). (d) Schematic representation of AuNP dimers, attached to the glass coverslip by biotin/Neutravidin, going from a stretched geometry to touching particles when the NaCl concentration is increased. Typical evolution of the scattering spectrum (e) and of the darkfield image (f) for a single dimer when the salt concentration is increased: 50 mM (red), 100 mM (black), 200 mM (purple), 400 mM (green), and 800 mM (blue).

DNA coverage of the AuNPs. Indeed, the amount of dimers obtained in lanes 9 and 10 is significantly larger than that in lane 7. Furthermore, the dimers obtained in column 10 have electrophoretic mobilities significantly lower than the ones in lanes 7 and 8, indicating that they feature a large amount of unhybridized DNA strands on the particle surfaces. The association of unreacted particles and available DNA strands on their surface demonstrates that the reaction is still in progress after a 12 h incubation time (lanes 7−10).

When comparing lanes with identical building blocks (for instance, lanes 6 and 10), we observe a strong increase in the production of groupings larger than dimers for a 10× larger incubation time. In particular, lane 6 features groupings that are too large to diffuse in the gel and practically no unreacted AuNPs. This evolution is much weaker when comparing lanes 3 and 7 for which the majority of particles stay unreacted and where only a dimer band is clearly visible. By comparing lanes 6 and 7, we observe that an 8× increase of the DNA concentration and a 10× increase of the reaction time turns the sample from isolated particles with a few dimers to large DNA-templated groupings. Overall, we observe, as in the case of 8 nm particles, that a weak (5×) excess of the **S**+**T** trithiolated strand leads to the formation of dimers preferentially linked by one DNA strand. Furthermore, the 2.5× larger excess of **C** means that most unreacted strands on the particle surface will not carry the structural information on the hairpin loop. In the following optical experiments, the studied dimers are obtained with the protocol followed in lane 7.

When comparing lanes 3−6 and 7−10, we also observe that the electrophoretic mobility of the groupings is lower after a longer incubation time. This can arise from the limited stability of the monothiolated ethylene glycol passivating layer on the particles that minimizes nonspecific interactions between the AuNPs and the agarose gel. This is why all optical experiments are performed within 1 week of the dimer synthesis and purification.

Darkfield Spectroscopy. Figure 1c shows a darkfield image of 40 nm AuNP dimers incubated in Neutravidin-coated microfluidic flow chambers in a Tris pH = 8 buffer solution containing 25 mM of NaCl. These groupings, obtained from lane 7, feature a double-stranded **S**+**T** scaffold, corresponding to an open hairpin loop, as represented on Figure 1d. Since dimers (circled in red) can be easily discriminated from single particles (blue circle) or larger groupings (example in

yellow) in these large fields of views,[15,19] it is possible to estimate the dimer purity, which is typically 80% in these experiments. The darkfield signal from isolated dimers can be spatially filtered using a 50 μm multimode fiber before reaching an imaging spectrometer to obtain a confocal scattering spectrum as shown on Figure 1e. This spectrum is dominated by the longitudinal plasmon resonance of the dimer.[5,15] For each dimer, we associate this spectrum to the darkfield image obtained on a low-cost color CCD camera, as shown on Figure 1f.

The longitudinal resonance wavelength of AuNP dimers is sensitive to the interparticle distance at the nanometer scale.[5,16] In DNA-templated groupings, the interparticle distance is strongly influenced by the repulsive electrostatic interactions between AuNPs and, therefore, on the concentration of Na^+ cations that screen them and reduce the persistence length of the DNA double strands.[10,15,20,28] At low ionic strengths, DNA-linked dimers feature a stretched geometry where the interparticle distance is in good agreement with the length of the DNA template and of the thiolated groups.[15,20] Figure 1d provides a schematic representation of a dimer going from a stretched shape to touching particles in the presence of cations.

When increasing the NaCl concentration in the buffer solution of the flow chamber by factors of 2 up to 800 mM, we observe in Figure 1e a strong red shift for the plasmon resonance of a given dimer from 555 to 600 nm. These measurements are performed after a short 10 min incubation time at each salt concentration. This resonance change cannot be accounted for from the small change in refractive index when increasing the salt concentration ($\Delta n < 8 \times 10^{-3}$) that, for 40 nm AuNP dimers with an initial resonance at 555 nm, would lead to a wavelength shift much lower than 1 nm.[15] The strong salt-induced red shift that is also clearly visible in the CCD images of Figure 1f is due to a reduction of the interparticle distance when repulsive electrostatic interactions are screened.

The progressive red shift observed in Figure 1e is the typical behavior observed in the studied dimers (about 60% of our measurements). Other common occurrences are given in Figure S2: a progressive red shift but with a secondary peak around 540 nm that could arise from a strong transverse mode (around 15%); a nearly constant resonance wavelength at low ionic strength that strongly red shifts at a high NaCl concentration (20%); finally, in a few cases (less than 5%), the resonance wavelength can blue shift or red shift when the salt concentration is increased, in a seemingly uncorrelated way. Measurements were performed on 50 different dimers. Because a few dimers detach from the surface or disassemble during the consecutive measurements, and because the longitudinal mode from several groupings cannot be properly fitted with a Lorentzian function to estimate the resonance wavelength, we perform a statistical analysis on 41 dimers in Figure 2a.

Parallel Morphological Analysis of Particle Dimers. Measurements associating the scattering spectrum of 40 nm AuNP dimers to their image on a color CCD camera were performed on several thousand groupings and allow us to properly calibrate the hue of the CCD HSV color space to a corresponding resonance wavelength. The calibration curve is obtained by plotting the resonance wavelength of dimers with respect to the average hue of the 185 pixels corresponding to their diffraction-limited image. Figure 2b is a 2D distribution of (hue, resonance wavelength) occurrences in logarithmic scale, estimated on 6460 measurements of single dimers. The (hue, resonance wavelength) occurrences are integrated over a Δhue of 0.02 and a $\Delta\lambda$ of 0.8 nm. The average resonance wavelength for a given hue $\pm$0.015 is given in Figure 2b with the standard error. This curve is fitted by a polynomial function (white solid line in Figure 2a) that we use as a calibration function to estimate single dimer resonance wavelengths from hue values measured on the color camera.

Using this phenomenological relationship, we compare in Figure 2d the average resonance wavelengths of the 41 aforementioned dimers, measured by confocal scattering spectroscopy, with the corresponding value estimated from the CCD hue at different salt concentrations. We observe a quantitative agreement within the experimental standard error. These curves are given as a logarithmic scale of the ionic strength because of the 2$\times$ increase in NaCl concentration between each consecutive measurement from 25 to 800 mM. Compared to confocal scattering spectroscopy or previously reported multispectral imaging techniques,[18] this hue-based approach does not require any scanning of the sample or of the excitation wavelength. Furthermore, it is compatible with low-cost color cameras. However, the calibrated relationship between the resonance wavelength and the CCD hue is only valid for 40 nm AuNP dimers or for samples with similar resonance line widths.

To translate the spectral measurements of Figure 2d into morphological information on the AuNP dimers, we use generalized Mie theory (GMT) calculations. A previous study of the scattering response from DNA-linked 36 nm diameter AuNP dimers with the same surface chemistry on Neutravidin-coated glass coverslips showed that GMT calculations with an average $n = 1.4$ dielectric environment were in good agreement with experimental plasmon resonance wavelengths.[15] The estimated evolution of the longitudinal resonance wavelength as a function of the surface-to-surface distance is given in Figure 2e for 39 nm gold spheres (corresponding to the average diameter of particles in this study), using the bulk refractive index of gold.[29]

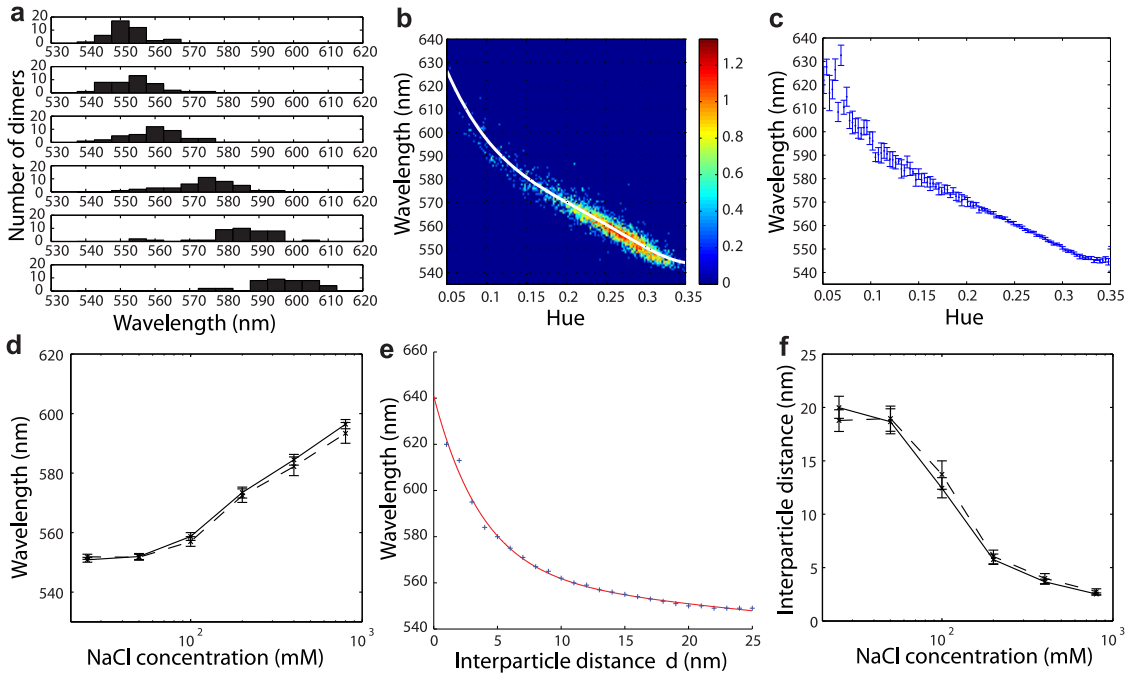

Figure 2. (a) Distribution of longitudinal resonance wavelengths for 40 nm AuNP dimers with an open S+T DNA scaffold at NaCl concentrations increasing, by factors of 2, from 25 to 800 mM (from top to bottom, bin width is 5 nm). (b) Distribution of (hue, resonance wavelength) occurrences in logarithmic scale with the calibration curve (white solid line). (c) Average resonance wavelength values for different hue estimations. Error bars correspond to the standard error. (d) Evolution of the average plasmon resonance wavelength when varying the salt concentration, using confocal scattering spectra (solid lines) or the calibrated CCD (dashed lines). (e) Theoretical evolution of the longitudinal plasmon resonance wavelength of 39 nm gold spheres estimated in generalized Mie theory for $n = 1.4$. The solid line is a biexponential fit. (f) Evolution of the estimated interparticle distances when varying the salt concentration, using confocal scattering spectra (solid lines) or the calibrated CCD (dashed lines). The error bar for the distance is obtained by estimating the spacing for the average wavelength plus or minus the standard wavelength error (see SI for details).

The numerical values are fitted by a biexponential function that we use as a calibration curve.

Using this relationship, we estimate average interparticle distances in Figure 2f from the measurements of Figure 2d. As discussed in previous studies,[15,20] the dimers feature stretched geometries at low ionic strengths (25−50 mM NaCl): the 20 nm initial interparticle distance is in good agreement with the 17.5 nm 50 bp DNA spacer added to the 2 nm width of the perpendicular DNA strand linking the two particles and the 1 nm long trithiolated moieties.

As the salt concentration is increased, we observe a progressive decrease of the interparticle distance with a quantitative agreement between spectral measurements performed in confocal spectroscopy and on the calibrated color camera. This demonstrates the possibility to measure in parallel, on a low-cost detector, the nanometer-scale distance between gold particles in a 3−20 nm range. The 3 nm estimated gap at 800 mM NaCl corresponds to the lengths of the surface chemistries on both particles. This indicates that, at high ionic strength, the interparticle distance is governed by the particle surface chemistry and seems independent of the linking DNA scaffold. Furthermore, since the lowest observed spacing corresponds to touching surface chemistries, the ethylene glycol passivating layer provides a good steric protection against aggregation in these experimental conditions with short incubation times.

Long-Term Stability of Gold Nanoparticle Groupings. To further understand the sensitivity of DNA-templated AuNP groupings to the local ionic strength, we analyze the evolution of the average resonance wavelength of dimers for increasing NaCl concentrations with long incubation times (10 h). In this case, we do not follow the evolution of the same subpopulation of dimers in one sample, as in Figure 2, but study different microfluidic chambers obtained with the same purified dimer suspension and left to incubate in different salt-containing buffer solutions. The histograms of resonance wavelengths measured by confocal scattering spectroscopy are given in Figure 3a, with a total of 524 dimers for all six measurements. We observe that, for NaCl concentrations larger than 200 mM, the longitudinal resonance wavelength can reach 680 nm. A typical scattering spectrum with such red-shifted resonances is given in Figure 3b; we observe the longitudinal mode at 682 nm along with the blue-shifted transverse mode around 547 nm.

The average resonance wavelengths estimated by confocal spectroscopy and with the calibrated CCD camera are given in Figure 3c along with the values obtained with a 10 min incubation time. The corresponding interparticle distances, estimated from

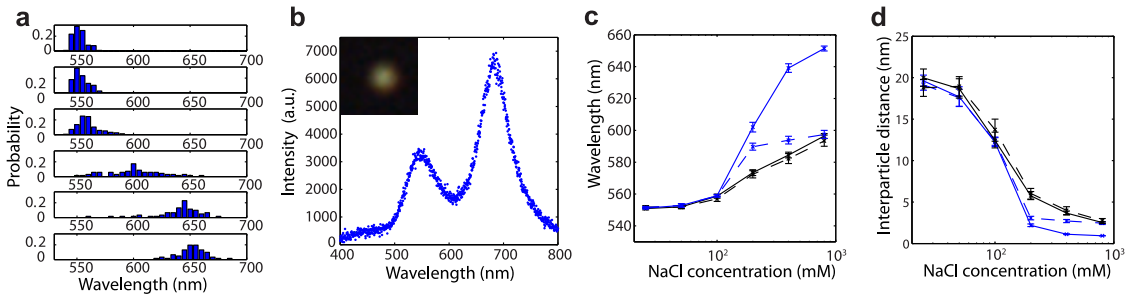

Figure 3. (a) Distribution of longitudinal resonance wavelengths for 40 nm AuNP dimers with an open S+T DNA scaffold at NaCl concentrations increasing, by factors of 2, from 25 to 800 mM after a 10 h incubation (from top to bottom, bin width is 5 nm). (b) Example of a scattering spectrum for an aggregated dimer with clearly separated transverse and longitudinal modes. Inset: image on the color CCD camera. Evolutions of the average plasmon resonance wavelength (c) and estimated interparticle distances (d) when varying the salt concentration with a 10 h (blue data) or a 10 min (black data) incubation time, using confocal scattering spectra (solid lines) or the calibrated CCD (dashed lines).

GMT calculations, are given in Figure 3d. We observe that, for NaCl concentrations lower than 100 mM, the measured resonance wavelengths and corresponding interparticle distances are independent of the incubation time. This indicates that AuNP dimers should be stable at these salt concentrations. However, we observe a drastic red shift of the optical responses when the ionic strength is larger, with interparticle spacings below 3 nm. For high NaCl concentrations, where the AuNPs are initially close to touching surface chemistries, interaction kinetics thus play an important role as the passivating ligands can interpenetrate at long incubation times. The estimated spacings then reach values close to 1 nm where our GMT calculations are not quantitative because of nonlocal effects.[30,31] We can however conclude that, with longitudinal resonance wavelengths around 650 nm, the dimers are irreversibly aggregated. This means that, when rinsing the microfluidic chamber with a low-salt containing buffer solution, the dimers maintain their sub-3 nm interparticle distance.

The 200 mM NaCl experiment appears to be a transition where only a limited number of dimers are aggregated with a large distribution of resonance wavelengths in Figure 3a. This is also the ionic strength above which the CCD hue does not provide a quantitative estimation of the plasmon resonance and, therefore, of the interparticle gap. We only observe qualitatively that an increased ionic strength leads to a resonance red shift and shorter particle gaps. In practice, the calibrated hue provides an underestimated wavelength and overestimated distance. This is due to the wavelength dependence of the detector quantum yield which is accounted for in confocal spectra (for instance in Figure 3b) but not in the CCD spectral estimation. Color CCDs are developed to have a sensitivity similar to the human eye: maximum around 500−550 nm and significantly weaker at 650 nm. In our case, the quantum yield for the longitudinal peak at 682 nm of Figure 3b is four times lower than for the transverse peak. This is why the CCD image features a mix of green and red. The validity of the CCD hue to estimate the plasmon resonance wavelength could be extended to red and near-infrared frequencies by using a nonstandard definition of the hue in which the intensity of the green pixels is corrected for the higher detector quantum yield at 500 nm or by using a deep-depleted camera with a weakly wavelength-dependent quantum yield over the visible to near-IR spectrum. Another possibility is to minimize scattering from the transverse mode using a polarization analysis.

Dimer Orientation and Interparticle Distance Imaging. Polarization-dependent scattering spectroscopy is a powerful tool to analyze the optical properties of AuNP dimers[8,9] but also more complex 2D and 3D AuNP groupings.[32] In our experimental conditions, the conjugation geometry of the AuNP dimers on Neutravidin-functionalized glass slides favors an out-of-plane orientation (see Figure 1d) because only one particle features biotin groups and the other has repulsive electrostatic interactions with the negatively charged albumin-coated surface. However, previous polarization-resolved measurements demonstrated that the particles have a partial in-plane orientation.[8,33] Furthermore, electrostatic repulsions are screened at high ionic strengths. By adding a polarizer in the detection path of the darkfield microscope, we indeed observe a strong in-plane optical anisotropy from the scattering response of a single aggregated dimer in Figure 4a. The imaged scattered light goes from green (corresponding to the transverse mode of the dimer) to red (longitudinal dimer mode).

We introduce a polarization filter in the collection and not the excitation path of the microscope because the high numerical aperture (NA) of the darkfield condenser, with an unpolarized white light, produces a complex combination of in-plane and out-of-plane polarizations on the sample. On the other hand, the low 0.6 NA collection objective ensures that the polarization analysis is only sensitive to the in-plane orientation of the AuNP dimers.

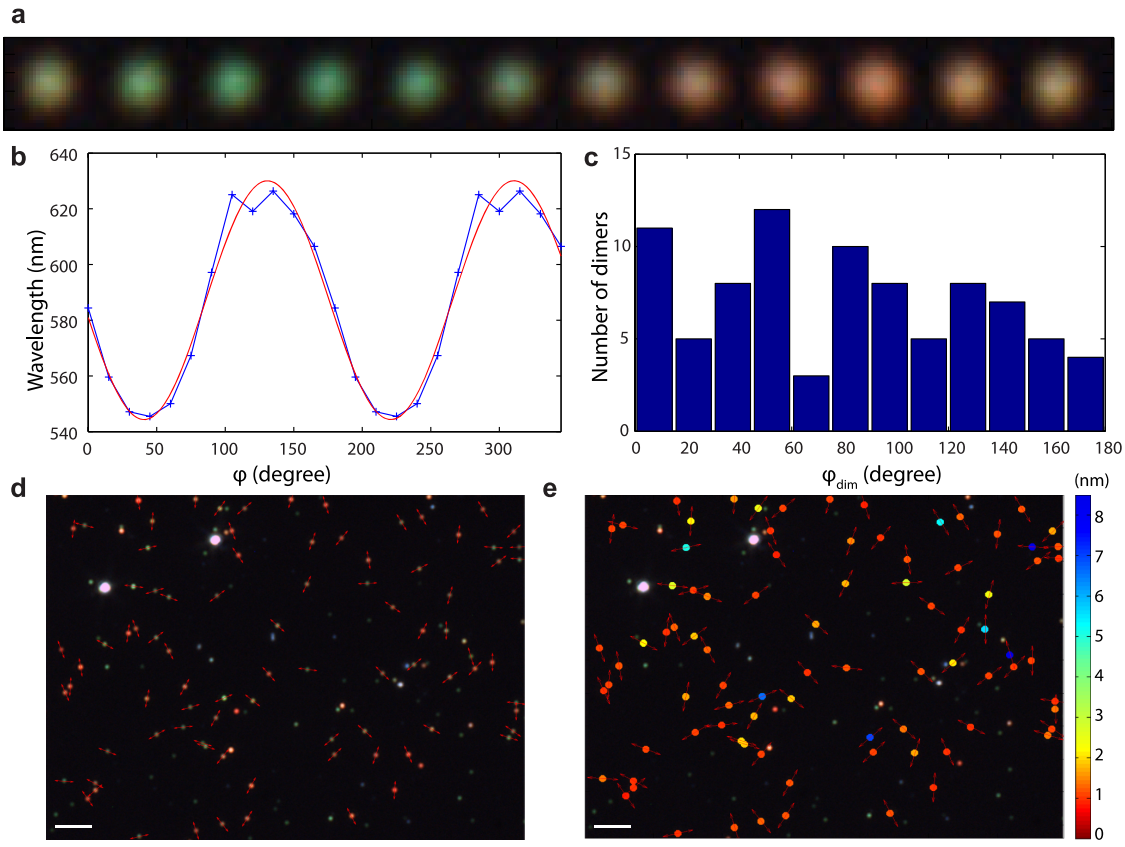

Figure 4. Evolution of the darkfield image (a) and of the CCD-estimated resonance wavelength (b) for a single aggregated dimer when changing the orientation of an analyzing polarizer every 15°, between 0 and 180° (the data are plotted twice in b for the cosine square fit). (c) Distribution of in-plane orientations of AuNP dimers after a 10 h incubation at 800 mM NaCl. Darkfield image of the dimer sample superimposed with the dimer in-plane orientation (*d*, represented as an arrow) and the interparticle distance (*e*, values in nm) estimated for each grouping (scale bar is 5 μm).

Figure 4b shows the effective wavelength estimated from the CCD hue with respect to the orientation φ of the analyzing polarizer. $\varphi = 0$ corresponds to the orientation of the liquid flow in the microfluidic chamber. This effective wavelength only corresponds to the resonance of the longitudinal and transverse modes when the polarizer is parallel or perpendicular to the in-plane axis of the AuNP dimer. For intermediate orientations, the effective wavelength only reflects the relative strengths of the two resonances. If φ_{dim} is the in-plane orientation of the dimer, then, in a dipolar approximation, the light intensity scattered by the longitudinal and transverse modes should have $\cos^2(\varphi - \varphi_{dim})$ and $\sin^2(\varphi - \varphi_{dim})$ dependencies, respectively.[34]

With I_L and I_T, the scattered intensities of the longitudinal and transverse modes collected by the microscope objective, respectively, the measured intensity should vary as $I_T + (I_L - I_T)\cos^2(\varphi - \varphi_{dim})$. In practice, we phenomenologically observe that this cosine square dependence of the intensity translates into a $\cos^2(\varphi - \varphi_{dim})$ variation of the hue-estimated wavelength that can be fitted to provide the in-plane orientation, φ_{dim}, of each dimer. In less than 15% of the studied groupings, we do not observe this cosine square dependence which can arise from the analysis of a trimer or from a strongly nonspherical particle in dimers. The histogram of in-plane orientations studied in 91 dimers is given in Figure 4c and indicates an isotropic distribution of dimer angles.

This polarization analysis of color CCD images thus provides both the in-plane orientation of the dimer and a good estimation of its longitudinal resonance. Figure 4d shows a darkfield image of 40 nm AuNP dimers incubated at 800 mM NaCl with a 10 h incubation time for a given polarizer orientation. On each grouping whose polarization-dependent hue could be fitted by a cosine function, we superimpose the in-plane dimer axis, indicating once more an isotropic orientation of the groupings. This shows that a parallel imaging of dimer orientations is possible with a simple color CCD and confirms the high dimer purity of our electrophoretically separated suspension of AuNP groupings.

The estimation of longitudinal resonance wavelengths also allows us to associate an interparticle distance to each dimer, as shown in Figure 4e. We observe that a widefield imaging of interparticle distances, even close to 1 nm, is possible with a calibrated color camera. Most dimers are aggregated with

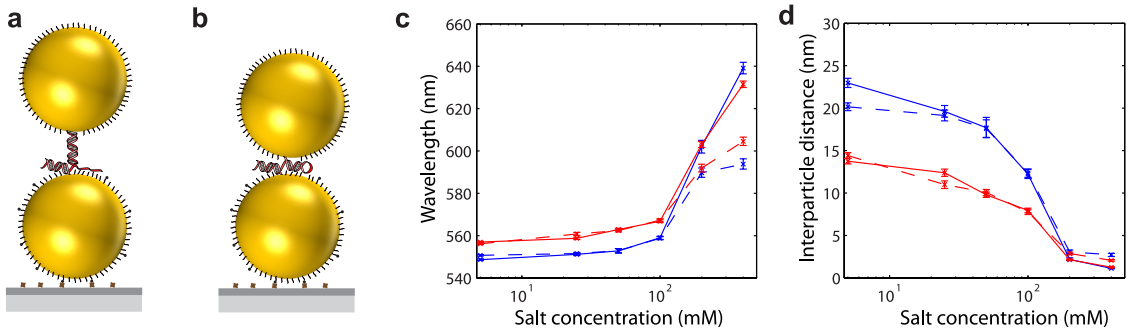

Figure 5. Schematic representations of open (a, S+T DNA scaffold) and closed (b, S strand alone) AuNP dimers. Evolutions of the average plasmon resonance wavelength (c) and estimated interparticle distances (d) for open dimers (blue data) and closed dimers (red data), when varying the NaCl concentration between 5 and 400 mM with a 10 h incubation time, using confocal scattering spectra (solid lines) or the calibrated CCD (dashed lines).

distances around 1 nm, while a subpopulation of groupings features spacings corresponding to partially interpenetrating surface chemistries (gaps between 2 and 3 nm). We also observe a few dimers with distances in a 6−8 nm range, indicating that nonspecific interactions with the substrate or the DNA scaffold limited the grouping distortion and did not allow the particles to touch.

In this measurement, the estimated interparticle distances are not fully quantitative for two reasons: variations of the AuNP diameter from one grouping to another are neglected and the electrodynamic GMT calculations do not account for nonlocal effects that occur for spacings below 1 nm.[30,31] However, this widefield polarization analysis provides information on the level and homogeneity of salt-induced particle aggregation in DNA-templated AuNP dimers.

Optical Characterization of the DNA Scaffold Conformation. As discussed previously, the morphology of DNA-linked gold particle dimers is very sensitive to the size of the biochemical scaffold at low ionic strength while, at high salt concentrations, the interparticle distance seems to be governed by the interaction of the AuNP surface chemistries. The applicability of these nanostructures as quantitative molecular rulers will therefore be strongly dependent on the experimental conditions. To prove that a simple widefield optical measurement allows the differentiation between dimers featuring two conformations of the same DNA template, we compare the results obtained above, for a fully hybridized scaffold, to measurements performed without the **T** single strand for which the hairpin loop in **S** should be closed. The geometries of the open and closed DNA-linked dimers are schematically given in Figure 5a,b.

AuNP dimers are synthesized following the same protocol used to obtain the groupings of column 7 in Figure 1a, except the nonbiotin featuring 40 nm particle is conjugated with the trithiolated **S** strand alone. It should therefore adopt a secondary hairpin loop architecture with a 20 bp stem. Figure 5c presents the evolution of the longitudinal resonance wavelength of closed dimers, measured on 852 groupings after a 10 h incubation time, at increasing salt concentrations, compared to the values obtained with an open scaffold. Using the same GMT data for 39 nm AuNPs in a $n = 1.4$ environment, we translate these spectral measurements in interparticle distances in Figure 5d.

We observe that the closed dimers follow a similar red-shifted variation of their resonance wavelength when increasing the ionic strength and aggregate for NaCl concentrations larger than 200 mM. Importantly, the samples provide significantly different optical responses for NaCl concentrations lower than 200 mM as verified in the confocal spectra. The resonance wavelength difference reaches 9.5 nm, corresponding to a 7.5 nm shorter interparticle distance, at 50 mM NaCl. Furthermore, the morphological difference is clearly visible on the calibrated CCD measurements, making the optical distinction possible in a simple widefield darkfield image.

For salt concentrations higher than 200 mM, it is not possible to optically differentiate dimers featuring a closed **S** or open **S**+**T** scaffold as the grouping morphology is governed by short-distance interactions between the AuNP surface chemistries and not the geometry of the DNA linker. As in Figure 3, the CCD estimation of the interparticle distances for aggregated dimers is underestimated because the transverse plasmon mode is visible on the measured hue.

Compared to interparticle distances measured in cryo-electron microscopy with 8 nm AuNPs at 50 mM NaCl with a similar DNA scaffold, we observe in Figure 5d longer spacings: while the 18 ± 1.5 nm optically estimated value for the open geometry is close to the 15.5 nm distance found in electron microscopy, the 10 ± 0.5 nm spacing for the closed DNA template is significantly larger than the previously reported 5.5 nm length.[20] This discrepancy probably arises from larger repulsive interparticle interactions with 40 nm AuNPs than with 8 nm particles, even though the same thiolated ethylene glycol surface chemistry is used in both experiments. In the case of dimers with the closed hairpin loop, these interactions

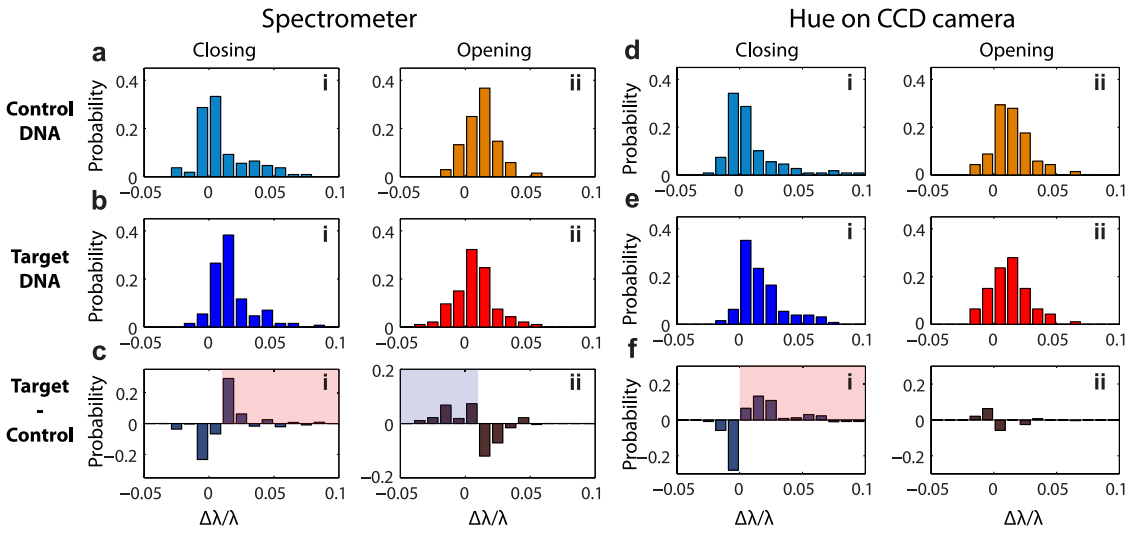

Figure 6. Distributions of relative resonance wavelength shifts $\Delta\lambda/\lambda$, after a 12 h incubation with a nonspecific reference (a,d) or target (b,e) DNA strand at 100 mM NaCl, for open (i) and closed (ii) 40 nm AuNP dimers. (c,f) Residues after subtracting the $\Delta\lambda/\lambda$ distribution for the reference strand to the distribution for the target strand: the red insets (respectively blue) highlight the higher probability of a spectral red shift when closing the dimer (respectively blue shift when opening the dimer). The optical measurements are performed at 5 mM NaCl before and after the incubation by confocal scattering spectroscopy (a−c) and with the calibrated CCD camera (d−f).

probably partially dehybridize the first base pairs of the 20 bp stem or of the second 50 bp double strand that links the particles. Therefore, even at a low ionic strength, the estimated dimer morphology does not directly translate the DNA sequence but is strongly sensitive to the physical chemistry of interparticle interactions in the experimental buffer conditions.

Parallel Optical Monitoring of the Closing and Opening of a DNA Hairpin. The results of Figure 5 demonstrate that the open and closed AuNP dimers can be easily discriminated in darkfield microscopy and spectroscopy. This difference in optical signals was recently used to sense specific target DNA sequences or proteins in complex biochemical samples using confocal scattering spectroscopy.[10,12,13] However, these sensors suffer from a low dimer purity in microfluidic samples (a few percent with mostly isolated particles), which limits the applicability of a fast parallel imaging approach.

In the AuNP dimers studied here, electrophoretic purification leads to microfluidic chambers consisting typically of 80% dimers and to nanostructures preferentially featuring one DNA strand with a hairpin loop linking the particles together. Furthermore, experiments performed with 8 nm gold particles showed that, with a small excess of target DNA strand compared to the nanostructure concentration, such DNA-templated dimers could be reversibly switched between open and closed configurations at room temperature in less than 30 min.[20] This switching behavior with small AuNPs was also shown to be sensitive to non-DNA targets (such as ATP) using an aptamer sequence in the scaffold.[35]

The label-free spectroscopic sensing of single biomolecules is possible in localized surface plasmon resonance spectroscopy using gold nanorods.[36,37] The surface attachment of a 450 kDa protein complex corresponds to a plasmon resonance shift lower than 0.3 nm, requiring complex confocal scattering[37] or photothermal[36] spectroscopies. The resonance wavelength variation of nearly 10 nm in Figure 5c, between open and closed geometries, is therefore appealing for the parallel label-free monitoring of single biomolecules with low-cost detectors. However, the long-term stability problems of DNA-linked AuNP dimers at high salt concentrations, raised in Figure 3, are an issue as cations are needed to screen the repulsion between the negatively charged DNA target and particle grouping (NaCl concentrations larger than 80 mM in reported experiments).[10,20,35]

Distributions of resonance wavelength variations $\Delta\lambda/\lambda$ for single open and closed dimers after incubation with a 1 μM solution of the target DNA strand are given in Figure 6, compared to experiments performed with a reference polythymine nonspecific strand. The spectral shifts are estimated both in confocal spectroscopy and with the calibrated color camera. To allow the hybridization of the **T** strand on **S** to open the hairpin loop, or the removal of the **T** strand from the **S**+**T** scaffold to close it by introducing the complementary sequence of **T**, we perform a 12 h incubation at 100 mM NaCl. To monitor a large spectral shift between the open and closed geometries, we perform confocal spectroscopy and darkfield imaging, before and after incubation, at a low 5 mM NaCl concentration after rinsing the flow chamber. Furthermore, we remove from the statistical analysis dimers for which the resonance wavelength does not red shift ($\Delta\lambda < 5$ nm) when changing the NaCl concentration from 5 to

100 mM, before incubation with the target or reference DNA strand, since they correspond to structures in which the nongrafted AuNP is not free in suspension. These nanostructures, which account for about 25% of the studied dimers, were already discussed with respect to Figure 1e (and Figure S2): their longitudinal resonance wavelength stays constant at low ionic strength but strongly increases for salt concentrations larger than 200 mM. Overall, the four distributions of Figure 6 were obtained by following the spectral evolution of 396 individual nanostructures.

We observe on Figure 6a(i) that, when an open AuNP dimer is incubated with a nonspecific reference single strand, a majority of nanostructures feature a stable resonance wavelength ($|\Delta\lambda| < 5$ nm). This confirms the results of Figure 3b, in which short and long incubation times below 100 mM NaCl resulted in similar average resonance wavelengths. Furthermore, by comparing the resonance wavelength shifts for this sample when increasing the salt concentration from 5 to 100 mM NaCl and when reducing it from 100 to 5 mM NaCl (after the 12 h incubation), we observe the reversibility of the salt-induced interparticle distance modification for nonaggregated dimers: the distribution of initial wavelength red shifts is similar to the final blue shifts (see Figure S4).

However, about 30% of groupings exhibit an overall significant spectral red shift in Figure 6a(i) after the 12 h incubation. This phenomenon can arise from two effects: a shortening of the interparticle distance due to the long incubation time at 100 mM NaCl and gravity but also an increase of the refractive index on the surface of AuNPs from nonspecific attachment of the DNA strand. These results indicate that, after a long incubation time at 100 mM NaCl, rinsing the sample with a 5 mM buffer solution does not allow all AuNP dimers to recover their initial interparticle distance even if the reference strand does not interact with the DNA template of the open dimers.

The nonspecific red shift of dimer resonances is much stronger for closed dimers, as shown in Figure 6a(ii), where more than 60% groupings feature a large increase of their resonance wavelength. This probably originates from the initially shorter interparticle distance that increases the effect of a change in spacing and/or of the surrounding dielectric index on the red shift of the plasmon resonance.

Figure 6b shows the resonance wavelength shift when open and closed AuNP dimers are incubated with the specific DNA sequences, allowing the closing and opening of the hairpin loop, respectively. Introduction of the strand complementary to **T** with open dimers leads to a red shift larger than 5 nm in 70% of the studied dimers. We ensure that the distributions of Figure 6a(i) and Figure 6b(i) are statistically different using the two-sided Wilcoxon rank-sum test and find a p value of 2×10^{-6} (well below the 0.05 threshold above which the distributions have equal medians).[38] Furthermore, by subtracting the reference distribution to the target measurement, we observe in Figure 6c(i) a much larger probability of observing a $\Delta\lambda \approx 10$ nm spectral shift with the target DNA sequence than with the reference nonspecific one. However, this larger red shift for the hairpin closing step only corresponds to 34% of the sample. This shows that even a 12 h incubation time at 100 mM NaCl with a high DNA concentration (1 μM) is insufficient for a complete reaction. The studied interaction is therefore kinetically unfavored in these experimental conditions.

The same experimental analysis is performed in Figure 6b(ii) and Figure 6c(ii) for the hairpin opening experiment. In the distribution of spectral shifts by incubating the **T** strand with closed dimers, we observe a weaker red shift than in the reference measurement. This is statistically verified with the Wilcoxon rank-sum test corresponding to a p value of 0.018. However, we observe that the expected blue shift due to the opening of a number of dimers is weaker than the red shift due to the aging of the sample after a 12 h incubation at 100 mM NaCl. In Figure 6c(ii), we observe that only 19% of the sample is blue-shifted with respect to the reference measurement. The fact that the hairpin opening reaction is more kinetically unfavored than the closing step (because of steric hindrance in closed dimers) was already observed in electrophoretic mobility measurements.[20]

Resonance wavelength shifts estimated with the calibrated color camera, shown in Figure 6d–f, show similar trends. In particular, the distributions corresponding to open dimers, when interacting with a reference or the target strand, are statistically different (p value of 7×10^{-8}) with 28% of studied dimers featuring a larger red shift for the specific closing reaction. This lower value, compared to confocal spectroscopy, indicates more experimental noise in the parallel measurement, but monitoring the reaction of a limited fraction of dynamic AuNP dimers is possible on a color CCD. This extra noise, associated with the lower number of reactive dimers for the hairpin opening reaction, means that the interaction of closed dimers with the **T** strand is not visible on the CCD measurement (p value of 0.042 close to the 0.05 threshold).

Overall, the DNA-templated AuNP dimers studied here are not optimized for sensing applications: they suffer from nonspecific spectral red shifts after long incubation at high salt concentrations (especially closed dimers); they feature spectral shifts of less than 10 nm when switching shape (value similar to the nonspecific red shift); and they suffer from low reaction kinetics. All these issues are related to the AuNP surface chemistry as it governs the stability of the dimer morphology at high ionic strength but also influences the length of the closed hairpin scaffold (that seems partially dehybridized from the spectral measurements)

and introduces steric hindrance around the recognition site, thus reducing the reactivity. Using a high coverage of the hairpin-containing DNA strand on the particle surface was reported in the literature,[10,12] but replacing the ethylene glycol passivating layer by a thiolated thymine hexamer did not provide a measurable increase of the dimer stability in our experiments.

Independently of the dimer stability and reactivity, the results of Figure 6 demonstrate that, with resonance wavelength shifts larger than 5 nm, a spectral widefield monitoring of conformational changes in single DNA-templated groupings is possible on a low-cost color camera at time scales of several hours.

CONCLUSION

The spectral analysis of the plasmon resonance of gold nanoparticle groupings allows quantitative information on nanometer-scale changes in interparticle distances. We demonstrate here that these measurements can be performed in parallel on a simple calibrated color camera in a 3−20 nm distance range. A polarization analysis extends this range to 1 nm distances in conjunction with the widefield estimation of in-plane dimer orientations.

Our experiments also discuss how the morphology of DNA-templated particle dimers varies at different ionic strengths for varying incubation times. At low salt concentrations, the geometry of AuNP dimers is sensitive to the length of the scaffold linking the particles in conjunction with repulsive electrostatic interactions, allowing the widefield discrimination of groupings with different DNA conformations. However, at high ionic strengths, the interparticle spacing is dominated by short distance interactions between the AuNP surface chemistries with touching and interpenetrated ligand shells for short and long incubation times, respectively.

The influence of charge-screening cations on the shape of AuNP dimers is an essential parameter for their applicability as molecular rulers and plasmon-based biosensors. The introduction of hydrophobicity on the ligand shell[39,40] and the use of more complex DNA scaffolds such as 3D origamis,[41,42] to optimize the stability and reactivity of these nanostructures, are potential directions to allow the quantitative widefield analysis, on low-cost detectors, of biomolecular conformations and single biochemical events using dynamic plasmon rulers.

METHODS

Synthesis of AuNP Dimers. Commercial 40 nm AuNPs (BBI, UK) are coated with a negatively charged phosphine ligand (BSPP, Strem Chemicals, USA) then rinsed and concentrated by centrifugation following published procedures.[15] The PAGE-purified trithiolated **S** (Fidelity Systems, USA) and unmodified **T** strands (IDT DNA, USA) are hybridized in 100 mM NaCl by heating the mix at 80 °C and leaving it to cool overnight. DNA-functionalized AuNPs are obtained by incubating 0.04 pmol 40 nm AuNPs with varying amounts of trithiolated **S**, **C**, or **S**+**T** strands in a 25 mM NaCl, 1.5 mM BSPP solution with a final volume of 10 μL. The minimum amount of thiolated strand is 0.2 pmol (respectively 0.5 pmol) for **S** and **S**+**T** (respectively for **C**) and is then increased four times by a factor of 2 in Figure 1a. The solution also contains 50 pmol of a nonspecific **L** strand, added to increase the AuNP suspension stability.

After an overnight incubation, the particles functionalized with **S** and **S**+**T** are incubated with a 700 000× excess of thiolated/methyl-terminated ethylene glycol hexamer (Polypure, Norway) for 30 min. The particles featuring the **C** strand are incubated with a 8:1 mix of the same ligand and a biotinylated/thiolated ethylene glycol hexamer (Polypure, Norway: the ligand is obtained as a disulfide which is cleaved by reacting with an excess of BSPP).[15] The samples are then purified by agarose gel electrophoresis (1.5% weight) in 0.5× Tris-borate EDTA buffer (Figure S1). The passivated DNA-functionalized AuNPs are cut from the gel and concentrated by centrifugation before being incubated overnight in stoichiometric amounts (**S**+**T** or **S** with **C** for open and closed dimers, respectively) in 30 mM NaCl. The obtained suspensions are once again purified by gel electrophoresis (1.5 wt %) and yield the dimer samples described in Figure 1a.

The DNA sequences are as follows:

S: 5′-trithiol-GGCTTACATGAGGAGCTTGCTTCTGCGAGAACACTCGCAGAAGCAAGCTC CTCTGCACGAAACCTGGACACCCCTAAGCAACTCCGTATCAGATGGGAACAGCA-3′

T: 5′-TACGATAGTGGTATGATCGCTAGATCCGCAAGAGGAGCTAGTTACCTTCACAGGA AGTATCCTAGCTCCTCATGTAAGCC-3′

C: 5′-TGCTGTTCCCATCTGATACGGAGTTGCTTAGGGGTGTCCAGGTTTCGTGC -trithiol-3′

L: 5′-TGTTCAGACTGGGGATTTTTTTTTTTTTTTTTTTTTTTTTTTTTTTTT-TTTTTTTTTTTTTTTT TTTTTTTTTTTTTTTTTTTTTTTTTTGACCTCG-CACTTAGT-3′

Optical Measurements. Home-made microfluidic chambers are prepared using freshly cleaned 25 mm square glass coverslips that are stacked together with two layers of parafilm featuring a square hole (about 10 mm sides). Two micropipette tips (GELoader, Eppendorf, USA) are introduced between the parafilm layers before melting them at 100 °C to produce a 20−40 μL flow chamber with a 250 μm height. Following published protocols,[6,15] the glass slides are functionalized with BSA-biotin (Sigma-Aldrich, USA) and Neutravidin (Thermo-Scientific, USA) before introducing the dimer suspension at a sub-nanomolar concentration (15 min incubation) and rinsing the chamber with 200 μL of a 10 mM Tris, 5 mM NaCl buffer solution (pH = 8) called T5.

The salt concentration in the chamber is modified to an x value by rinsing the chamber twice with a Tx solution. Hairpin opening and closing experiments are performed by first rinsing the T5 chamber with T100 before incubating the closed (respectively open) dimers with 1 μM **T** (respectively the strand complementary to **T**) in T100 for 12 h. The chamber is rinsed with T100 and then T5. Reference measurements are performed with the same protocol but substituting the nonspecific **L** strand to the target sequences.

Darkfield images and spectra are measured in an inverted microscope (IX71, Olympus) coupled to a color CCD (Quicam, Roper) and to a fiber-coupled (50 μm core diameter) imaging spectrometer (Acton SP300 with Pixis 100 CCD detector, Princeton Instruments). White light from a 100 W halogen lamp is focused on the sample using an oil-immersion 1.2−1.4 NA darkfield condenser. Scattered light is collected with a 100× q0.6 NA oil-immersion objective. All color images are obtained with a 500 ms acquisition time (see Figure 1c). Using a built-in function of the Matlab software package, we convert the RGB color maps of the CCD camera in HSV color maps.

To measure several scattering spectra in parallel (typically up to 10), the center of each AuNP grouping, with respect to the

equivalent position of the fiber in the sample plane, is estimated on the color CCD image. The piezoelectric stage on which the sample is placed (P562-3CD, PI) is then programmed to align successively each grouping on the confocal detection volume of the fiber in order to measure a raw spectrum with a 5 s acquisition time. A background spectrum is measured with the same acquisition time on an empty area of the sample. The background is subtracted to the measured spectra before correction according to the wavelength-dependent illumination and detection (Figure 1e). For measurements with short incubation times and for hairpin closing and opening experiments, the scattering spectra are measured on the same dimers after modification of the chemical environment.

Conflict of Interest: The authors declare no competing financial interest.

Acknowledgment. The authors thank E. Larquet for the cryo-EM measurement, as well as B. Rolly, B. Stout and N. Bonod for the Mie theory data. This work was supported by Agence Nationale de la Recherche via project ANR 11 JS10 002 01, by LABEX WIFI (Laboratory of Excellence within the French Program "Investments for the Future") under references ANR-10-LABX-24 and ANR-10-IDEX-0001-02 PSL*, and by Region Ile-de-France in the framework of DIM Nano-K.

Supporting Information Available: Complementary data on AuNP dimer synthesis and optical measurements. This material is available free of charge *via* the Internet at http://pubs.acs.org.

REFERENCES AND NOTES

1. Elghanian, R.; Storhoff, J. J.; Mucic, R. C.; Letsinger, R. L.; Mirkin, C. A. Selective Colorimetric Detection of Polynucleotides Based on the Distance-Dependent Optical Properties of Gold Nanoparticles. *Science* **1997**, *277*, 1078–1081.
2. Storhoff, J. J.; Elghanian, R.; Mucic, R. C.; Mirkin, C. A.; Letsinger, R. L. One-Pot Colorimetric Differentiation of Polynucleotides with Single Base Imperfections Using Gold Nanoparticle Probes. *J. Am. Chem. Soc.* **1998**, *120*, 1959–1964.
3. Liu, J. W.; Lu, Y. Fast Colorimetric Sensing of Adenosine and Cocaine Based on a General Sensor Design Involving Aptamers and Nanoparticles. *Angew. Chem., Int. Ed.* **2006**, *45*, 90–94.
4. Sonnichsen, C.; Reinhard, B. M.; Liphardt, J.; Alivisatos, A. P. A Molecular Ruler Based on Plasmon Coupling of Single Gold and Silver Nanoparticles. *Nat. Biotechnol.* **2005**, *23*, 741–745.
5. Reinhard, B. M.; Siu, M.; Agarwal, H.; Alivisatos, A. P.; Liphardt, J. Calibration of Dynamic Molecular Rulers Based on Plasmon Coupling between Gold Nanoparticles. *Nano Lett.* **2005**, *5*, 2246–2252.
6. Reinhard, B. M.; Sheikholeslami, S.; Mastroianni, A.; Alivisatos, A. P.; Liphardt, J. Use of Plasmon Coupling to Reveal the Dynamics of DNA Bending and Cleavage by Single EcoRV Restriction Enzymes. *Proc. Natl. Acad. Sci. U.S.A.* **2007**, *104*, 2667–2672.
7. Skewis, L. R.; Reinhard, B. M. Spermidine Modulated Ribonuclease Activity Probed by RNA Plasmon Rulers. *Nano Lett.* **2008**, *8*, 214–220.
8. Wang, H. Y.; Reinhard, B. M. Monitoring Simultaneous Distance and Orientation Changes in Discrete Dimers of DNA Linked Gold Nanoparticles. *J. Phys. Chem. C* **2009**, *113*, 11215–11222.
9. Morimura, H.; Tanaka, S. I.; Ishitobi, H.; Mikami, T.; Kamachi, Y.; Kondoh, H.; Inouye, Y. Nano-analysis of DNA Conformation Changes Induced by Transcription Factor Complex Binding Using Plasmonic Nanodimers. *ACS Nano* **2013**, *7*, 10733–10740.
10. Chen, J. I. L.; Chen, Y.; Ginger, D. S. Plasmonic Nanoparticle Dimers for Optical Sensing of DNA in Complex Media. *J. Am. Chem. Soc.* **2010**, *132*, 9600–9601.
11. Verdoold, R.; Gill, R.; Ungureanu, F.; Molenaar, R.; Kooyman, R. P. N. Femtomolar DNA Detection by Parallel Colorimetric Darkfield Microscopy of Functionalized Gold Nanoparticles. *Biosens. Bioelectron.* **2011**, *27*, 77–81.
12. Chen, J. I. L.; Durkee, H.; Traxler, B.; Ginger, D. S. Optical Detection of Protein in Complex Media with Plasmonic Nanoparticle Dimers. *Small* **2011**, *7*, 1993–1997.
13. Guo, L. H.; Ferhan, A. R.; Chen, H. L.; Li, C. M.; Chen, G. N.; Hong, S.; Kim, D. H. Distance-Mediated Plasmonic Dimers for Reusable Colorimetric Switches: A Measurable Peak Shift of More Than 60 nm. *Small* **2013**, *9*, 234–240.
14. Tajon, C. A.; Seo, D.; Asmussen, J.; Shah, N.; Jun, Y. W.; Craik, C. S. Sensitive and Selective Plasmon Ruler Nanosensors for Monitoring the Apoptotic Drug Response in Leukemia. *ACS Nano* **2014**, *8*, 9199–9208.
15. Busson, M. P.; Rolly, B.; Stout, B.; Bonod, N.; Larquet, E.; Polman, A.; Bidault, S. Optical and Topological Characterization of Gold Nanoparticle Dimers Linked by a Single DNA Double Strand. *Nano Lett.* **2011**, *11*, 5060–5065.
16. Jain, P. K.; Huang, W. Y.; El-Sayed, M. A. On the Universal Scaling Behavior of the Distance Decay of Plasmon Coupling in Metal Nanoparticle Pairs: A Plasmon Ruler Equation. *Nano Lett.* **2007**, *7*, 2080–2088.
17. Rong, G. X.; Wang, H. Y.; Skewis, L. R.; Reinhard, B. M. Resolving Sub-diffraction Limit Encounters in Nanoparticle Tracking Using Live Cell Plasmon Coupling Microscopy. *Nano Lett.* **2008**, *8*, 3386–3393.
18. Wu, L. X.; Reinhard, B. M. Probing Subdiffraction Limit Separations with Plasmon Coupling Microscopy: Concepts and Applications. *Chem. Soc. Rev.* **2014**, *43*, 3884–3897.
19. Lee, Y. K.; Kim, S.; Oh, J. W.; Nam, J. M. Massively Parallel and Highly Quantitative Single-Particle Analysis on Interactions between Nanoparticles on Supported Lipid Bilayer. *J. Am. Chem. Soc.* **2014**, *136*, 4081–4088.
20. Lermusiaux, L.; Sereda, A.; Portier, B.; Larquet, E.; Bidault, S. Reversible Switching of the Interparticle Distance in DNA-Templated Gold Nanoparticle Dimers. *ACS Nano* **2012**, *6*, 10992–10998.
21. Zanchet, D.; Micheel, C. M.; Parak, W. J.; Gerion, D.; Alivisatos, A. P. Electrophoretic Isolation of Discrete Au Nanocrystal/DNA Conjugates. *Nano Lett.* **2001**, *1*, 32–35.
22. Zanchet, D.; Micheel, C. M.; Parak, W. J.; Gerion, D.; Williams, S. C.; Alivisatos, A. P. Electrophoretic and Structural Studies of DNA-Directed Au Nanoparticle Groupings. *J. Phys. Chem. B* **2002**, *106*, 11758–11763.
23. Aldaye, F. A.; Sleiman, H. F. Dynamic DNA Templates for Discrete Gold Nanoparticle Assemblies: Control of Geometry, Modularity, Write/Erase and Structural Switching. *J. Am. Chem. Soc.* **2007**, *129*, 4130–4131.
24. Bidault, S.; de Abajo, F. J. G.; Polman, A. Plasmon-Based Nanolenses Assembled on a Well-Defined DNA Template. *J. Am. Chem. Soc.* **2008**, *130*, 2750–2751.
25. Mastroianni, A. J.; Claridge, S. A.; Alivisatos, A. P. Pyramidal and Chiral Groupings of Gold Nanocrystals Assembled Using DNA Scaffolds. *J. Am. Chem. Soc.* **2009**, *131*, 8455–8459.
26. Li, H. X.; Rothberg, L. Colorimetric Detection of DNA Sequences Based on Electrostatic Interactions with Unmodified Gold Nanoparticles. *Proc. Natl. Acad. Sci. U.S.A.* **2004**, *101*, 14036–14039.
27. Li, Z.; Jin, R. C.; Mirkin, C. A.; Letsinger, R. L. Multiple Thiol-Anchor Capped DNA–Gold Nanoparticle Conjugates. *Nucleic Acids Res.* **2002**, *30*, 1558–1562.
28. Park, S. J.; Lazarides, A. A.; Storhoff, J. J.; Pesce, L.; Mirkin, C. A. The Structural Characterization of Oligonucleotide-Modified Gold Nanoparticle Networks Formed by DNA Hybridization. *J. Phys. Chem. B* **2004**, *108*, 12375–12380.
29. Johnson, P. B.; Christy, R. W. Optical Constants of the Noble Metals. *Phys. Rev. B* **1972**, *6*, 4370–4379.
30. Ciraci, C.; Hill, R. T.; Mock, J. J.; Urzhumov, Y.; Fernandez-Dominguez, A. I.; Maier, S. A.; Pendry, J. B.; Chilkoti, A.; Smith, D. R. Probing the Ultimate Limits of Plasmonic Enhancement. *Science* **2012**, *337*, 1072–1074.
31. Scholl, J. A.; Garcia-Etxarri, A.; Koh, A. L.; Dionne, J. A. Observation of Quantum Tunneling between Two Plasmonic Nanoparticles. *Nano Lett.* **2013**, *13*, 564–569.

32. Barrow, S. J.; Wei, X. Z.; Baldauf, J. S.; Funston, A. M.; Mulvaney, P. The Surface Plasmon Modes of Self-Assembled Gold Nanocrystals. *Nat. Commun.* **2012**, *3*, 1275.
33. Busson, M. P.; Bidault, S. Selective Excitation of Single Molecules Coupled to the Bright Mode of a Plasmonic Cavity. *Nano Lett.* **2014**, *14*, 284–288.
34. Mertens, H.; Biteen, J. S.; Atwater, H. A.; Polman, A. Polarization-Selective Plasmon-Enhanced Silicon Quantum-Dot Luminescence. *Nano Lett.* **2006**, *6*, 2622–2625.
35. Xu, P. F.; Hung, A. M.; Noh, H.; Cha, J. N. Switchable Nanodumbbell Probes for Analyte Detection. *Small* **2013**, *9*, 228–232.
36. Zijlstra, P.; Paulo, P. M. R.; Orrit, M. Optical Detection of Single Non-absorbing Molecules Using the Surface Plasmon Resonance of a Gold Nanorod. *Nat. Nanotechnol.* **2012**, *7*, 379–382.
37. Ament, I.; Prasad, J.; Henkel, A.; Schmachtel, S.; Sonnichsen, C. Single Unlabeled Protein Detection on Individual Plasmonic Nanoparticles. *Nano Lett.* **2012**, *12*, 1092–1095.
38. Hollander, M.; Wolfe, D. A.; Chicken, E. *Nonparametric Statistical Methods*; John Wiley & Sons: New York, 2013.
39. Kanaras, A. G.; Kamounah, F. S.; Schaumburg, K.; Kiely, C. J.; Brust, M. Thioalkylated Tetraethylene Glycol: A New Ligand for Water Soluble Monolayer Protected Gold Clusters. *Chem. Commun.* **2002**, 2294–2295.
40. Larson, T. A.; Joshi, P. R.; Sokolov, K. Preventing Protein Adsorption and Macrophage Uptake of Gold Nanoparticles *via* a Hydrophobic Shield. *ACS Nano* **2012**, *6*, 9182–9190.
41. Dietz, H.; Douglas, S. M.; Shih, W. M. Folding DNA into Twisted and Curved Nanoscale Shapes. *Science* **2009**, *325*, 725–730.
42. Acuna, G. P.; Müller, F. M.; Holzmeister, P.; Beater, S.; Lalkens, B.; Tinnefeld, P. Fluorescence Enhancement at Docking Sites of DNA-Directed Self-Assembled Nanoantennas. *Science* **2012**, *338*, 506–510.